行政院國家科學委員會補助專題研究計畫■成果報告
□期中進度報告

氧化鈣含量對氧化鈣/氧化鋁系陶瓷材料與鈦金屬高溫擴散介面反應的影響

計畫類別：■ 個別型計畫　□ 整合型計畫
計畫編號：NSC 98-2221-E-009-039-MY2
執行期間：2009 年 8 月 1 日至 2011 年 7 月 31 日

計畫主持人： 林健正
共同主持人：
計畫參與人員： 呂明慰

成果報告類型(依經費核定清單規定繳交)：□精簡報告　■完整報告

本成果報告包括以下應繳交之附件：
□赴國外出差或研習心得報告一份
□赴大陸地區出差或研習心得報告一份
□出席國際學術會議心得報告及發表之論文各一份
□國際合作研究計畫國外研究報告書一份

處理方式：除產學合作研究計畫、提升產業技術及人才培育研究計畫、列管計畫及下列情形者外，得立即公開查詢
□涉及專利或其他智慧財產權，□一年□二年後可公開查詢

執行單位：國立交通大學材料工程與科學系所

中　華　民　國 99 年 8 月 5 日

Microstructural Characterization and Phase Formation Mechanisms at the Interface between Titanium and Ceria/Zirconia Ceramics at 1550˚C

Yao-Wen Chang and Chien-Cheng Lin
Department of Materials Science and Engineering, National Chiao Tung University, Hsinchu 30050, Taiwan

Abstract

Various CeO_2/ZrO_2 samples were fabricated by sintering, whereby CeO_2 was completely dissolved or reacted with ZrO_2 as a solid solution or $Ce_2Ze_3O_{10}$ and $Ce_2Ze_2O_7$ ternary compounds. Sintered samples were allowed to react with Ti at 1550°C for 4 h in argon. Microstructural characterization was conducted using x-ray diffraction and analytical electron microscopy. The CeO_2/ZrO_2 samples became more stable with increasing CeO_2 because CeO_2 was hardly reacted and dissolved in Ti. The incorporation of more than 50 mol% CeO_2 could effectively suppress the interfacial reactions in the Ti side, where relatively a small amount of β'-Ti(Zr, O) was found. Moreover, the content of O in α-Ti(O) far away from the interface was significantly decreasing with increasing amounts of CeO_2. Because CeO_2 was hardly dissolved into Ti, it completely remained in the residual ZrO_2, leading to the formation of spherical and worm-like $Ce_2Ze_3O_{10}$ in the outermost 10 mol% CeO_2 -ZrO_2 sample. In the outermost 30-50 mol% CeO_2 -ZrO_2 samples, $Ce_2Ze_2O_7$ was formed due to the outward diffusion of O and Zr away from $Ce_2Ze_3O_{10}$ into Ti. CeO_2 re-precipitated in the samples containing 50-70 mol% CeO_2, because the solubility of CeO_2 in Ti was

quite limited. On the ceramic side far from the original interface, spherical α-Zr and ZrO_{2-x} were formed in the 10 mol% CeO_2 -ZrO_2 sample. $Ce_2Zr_2O_7$ was formed in addition to residual ZrO_{2-x} in the 30 mol% CeO_2 -ZrO_2 sample. Dense α-Zr grains existed along the grain boundaries of the $Ce_2Zr_2O_7$ matrix in the 50 mol% CeO_2 -ZrO_2 sample. In the 70 mol% CeO_2 -ZrO_2 sample, free CeO_2 existed in the $Ce_2Zr_2O_7$ matrix. However, CeO was found in the sample containing 100 mol% CeO_2.

I. Introduction

High specific strength and good corrosion resistance have led to the large-scale use of titanium in the aerospace and chemical processing industries. However, they are extremely reactive to ceramics at high temperatures, resulting in chemical reaction affected-surface. The interfacial reactions between titanium and ceramics play an important role in the titanium precision casting. The interstitial elements (e.g., C, N, O, H) from the ceramic mold have a great tendency to enter into the titanium alloys during casting and cause the deterioration of mechanical properties.

Many researches[1-5] have been working on the reactions of the titanium with various ceramic molds or crucibles in the last few decades. Weber *et al*.[1] presented an unspecified feather-like eutectic phase in the reaction zone of Ti and MgO-ZrO_2 crucible. Ruh[2] found that zirconium entered the titanium lattice substitutionally and oxygen went to interstitial positions during the reactions between zirconia and titanium at elevated temperatures. While previous studies had been focused on the reactions taking place in the metal side, the transformation in the ceramic side had not been well attended. Thus,

the role of the ceramic mold in the interfacial reactions has not been fully understood to date.

Recently, Lin and his colleagues[6-12] have thoroughly investigated the phase formation mechanisms and microstructural evolution at the interface between titanium (or titanium alloys) and 3Y-ZrO_2 (or various ratios of Y_2O_3/ZrO_2) using analytical electron microscopy. The α-Ti(O), β'-Ti(Zr, O) and/or Ti_2ZrO were formed near the original interface due to the dissolution of ZrO_2 into Ti. Both lamellar orthorhombic Ti_2ZrO and spherical hexagonal Ti_2ZrO were found in α-Ti(Zr, O) after reaction at 1550°C.[8] Lin and Lin[9] also found the intergranular α-Zr, twinned *t*'-ZrO_{2-x}, lenticular *t*-ZrO_{2-x}, and/or ordered *c*-ZrO_{2-x} in the zirconia side far from the interface between Ti and 3Y-ZrO_2 after reaction at 1550°C. Concerning the reaction of Ti melt with various Y_2O_3/ZrO_2 samples at 1700°C,[12] the incorporation of more than 30 vol% Y_2O_3 in ZrO_2 could effectively suppress the reactions in the Ti side where only a very small amount of α-Ti and β'-Ti was found. Y_2O_3 re-precipitated in the samples containing 30-70 vol% Y_2O_3, because the solubility of Y_2O_3 in Ti was very low.

Several recent publications[13-15] have reported the importance of ceramic materials based on solid solutions of the ZrO_2–CeO_2 system, mainly those formulated in the ZrO_2–rich region. There are many potential applications of these materials, such as a toughened ceramic material in view of the existence of a relatively wide field of the tetragonal zirconia solid solution in the system ZrO_2–CeO_2. It is well known that ceria-doped zirconia polycrystals (Ce-TZP) exhibit high transformation toughness, even when compared to Y-TZP ceramics.[13-17] However, CeO_2 was cheaper than Y_2O_3. The ceria partially stabilized zirconia

has been considered as one of the most important industry ceramic material because of its good fracture toughness.

At present study, various ratios of CeO_2/ZrO_2 samples were attempted to achieve better control over the reactions on the titanium side as well as the ceramic side. The powder mixtures of CeO_2/ZrO_2 were sintered and then allowed to react with titanium at 1550°C for 4 h in argon. Various reaction layers at the interface between titanium and CeO_2/ZrO_2 samples were characterized using analytical scanning electron microscopy and analytical transmission electron microscopy. Finally, we would attempt to elucidate the effect of CeO_2 on the interfacial reactions between Ti and CeO_2/ZrO_2 samples.

II. Experimental Procedures

Starting powders used were zirconia (> 99.95 wt% ZrO_2+HfO_2 with HfO_2 accounting for approximately 2%-3% of this total, < 0.02 wt% Fe_2O_3, < 0.02 wt% TiO_2, < 0.004 wt% SiO_2, < 0.004 wt% Al_2O_3, < 0.002 wt% CaO; 0.5 μm in average; Toyo Soda Mfg. Co., Ltd. Tokyo, Japan), cercia (> 99.9 wt% CeO_2, < 0.04 wt% CaO, < 0.03 wt% SiO_2, < 0.02 wt% Fe_2O_3, < 0.01 wt% Na_2O_3; 0.5 μm in average; NYC, Ltd., Fukuoka, Japan).

The CeO_2/ZrO_2 samples contained 10, 30, 50, 70, and 100 mol% CeO_2, respectively, and were balanced with ZrO_2. The sample consisting of 10 mol% CeO_2 and 90 mol% ZrO_2 was designated as 10Ce90Zr, and so on. Powder mixtures were dispersed in ethanol. The pH of the suspension was adjusted to 11 by adding NH_4OH. The suspension was ultrasonically vibrated for 10 minutes (Model XL-2020, Sonicator, Heat Systems Inc., Farmingdale, NY), dried in an oven at 150°C, ground with

an agate mortar and pestle, and then screened through 80 mesh. The powder mixtures of CeO_2 and ZrO_2 were pressed into disks (20 mm in diameter x 5 mm thick) at a pressure of 200MPa and then sintered in air at 1400°C for 4 h at 5°C/min heating rate (Lindberg/Blue M STF54454C, Thermo Fisher Scientific Inc., Waltham Massachusetts, USA). Thereafter, the furnace cooled down to room temperature.

The apparent densities of CeO_2/ZrO_2 powder mixtures were measured using a gas pycnometer (Model MultiVolume Pycnometer 1305, Micromeritics, Norcross, GA) with 99.99% pure helium. The bulk densities of sintered samples were determined using the Archimedes method. The relative densities of the sintered samples were calculated as follows: Relative density = (bulk density/true density) × 100%. For a non-porous powder, the apparent density approximates the true density and can be used as the reference point in calculating the relative density. The designations, compositions, sintering conditions, and relative densities of CeO_2/ZrO_2 samples are listed in Table I.

Commercially pure titanium plates (99.7% purity, Alfa Aesar, Ward Hill, MA) were brought to react with various sintered CeO_2/ZrO_2 samples at 1550°C for 4 h in argon. Firstly, bulk CeO_2/ZrO_2 samples and titanium plates were cut and machined to dimensions of 10 × 10 × 4 mm. Their surfaces were ground and polished with a diamond paste, and then ultrasonically cleaned in acetone. One titanium disc was inserted in between two pieces of each CeO_2/ZrO_2 sample to produce a sandwiched type, and then put in the graphite furnace mentioned above, which was preparatorily pressed under 5 MPa, evacuated to 2×10^{-4} Torr, and filled with argon to one atmospheric pressure. This cycle of evacuation and purging was repeated at least three times. The temperature was raised

to 1000°C at a heating rate of 30°C/min, to 1550°C at 25°C/min, and then held at 1550°C for 4 h. Thereafter, the temperature was lowed to 1000°C at a cooling rate of 25°C/min, and then the furnace cooled down to room temperature.

The phase identification of the sintered CeO_2/ZrO_2 samples was performed using an x-ray diffractometer (XRD, Model MXP18, Mac Science, Yokohama, Japan). The operating conditions of x-ray diffraction were Cu K_α radition at 50 kV and 150 mA, and a scanning rate of 2 degrees/min.

A scanning electron microscope (SEM, Model JSM 6500F, JEOL Ltd., Tokyo, Japan) equipped with an energy dispersive x-ray spectrometer (EDS, Model ISIS 300, Oxford Instrument Inc., London, UK) was used for the microstructural observation on the interfaces between Ti and various CeO_2/ZrO_2 samples. Cross-sectional SEM specimens were cut and ground using standard procedures and finally polished using diamond pastes of 6, 3, and 1 μm in sequence.

The cross-sectional TEM specimens of the interfaces between Ti and various CeO_2/ZrO_2 samples were prepared by two different methods. Firstly, they were cut perpendicular to the interface and then polished, dimpled, and subsequently ion-beam-thinned using a precision ion-polishing system (PIPS, Model 691, Gatan, San Francisco, CA). The details of this traditional technique for preparing cross-sectional TEM specimens were described in a previous study.[12] Secondly, the TEM samples were acquired by an innovative technique. A specific location on a metallographic sample was ion-bombarded using a focused ion beam (FIB, Model Nova 200, FEI Co., Hillsboro, OR). The FIB

operating parameters were adjusted so that the electron beam was 5 kV from 98 pA to 1.6 nA and the ion beam was 30 kV from 10 pA to 7 nA. A TEM specimen with a thickness less than 100 nm was electron-transparent. The final TEM specimen was approximately 12 x 5 x 0.05 μm in size.

The interfacial microstructures were then characterized using a transmission electron microscope (TEM, Model JEM 2100, JEOL Ltd., Tokyo, Japan) equipped with an energy dispersive x-ray spectrometer (EDS, Model ISIS 300, Oxford Instrument Inc., London, UK). Analyses of atomic configurations in various phases were performed using computer simulation software for crystallography (CaRIne Crystallography 3.1, Divergent S.A., France). Chemical quantitative analyses for various phases were conducted by the Cliff-Lorimer standardless technique.[18] A conventional ZAF correction was operated using the LINK ISIS software.

III. Results and Discussion

(1) XRD analyses

Figure 1 shows the x-ray diffraction spectra of various CeO_2/ZrO_2 samples as well as pure CeO_2 after sintering. These spectra were arranged for CeO_2, 70Ce30Zr, 50Ce50Zr, 30Ce70Zr, and 10Ce90Zr, respectively, in a sequence from top to bottom. X-ray phases of these sintered CeO_2/ZrO_2 samples are summarized in Table I. In the 10Ce90Zr, all of the CeO_2 went into solid solution in zirconia such that only *t*-ZrO_2 and *m*-ZrO_2 were detected. Both of the 30Ce70Zr and 50Ce50Zr, *c*-ZrO_2, *t*-ZrO_2, tetragonal $Ce_2Zr_3O_{10}$,[19-21] and cubic $Ce_2Ze_2O_7$[22,23] were found. As for the 70Ce30Zr, $Ce_2Ze_2O_7$ and only cubic ZrO_2 phase were detected. In other words, the cubic ZrO_2 was

fully stabilized in 70Ce30Zr. While the content of CeO_2 was increasing from 30Ce70Zr to 50Ce50Zr, the amount of $Ce_2Ze_2O_7$ was significantly gradually increasing and the decreasing content of $Ce_2Zr_3O_{10}$. In the 100Ce, only cubic CeO_2 was detected. In general, CeO_2 was mutually dissolved or reacted with ZrO_2 as a solid solution or $Ce_2Zr_3O_{10}$ and $Ce_2Ze_2O_7$ compounds in various sintered CeO_2/ZrO_2 samples. The $Ce_2Ze_2O_7$ was formed due to the reduction of Ce^{+4} ions to Ce^{+3} in ZrO_2 with low oxygen partial pressure and Ce_2O_3 reacted with ZrO_2 as a 1:2 $Ce_2O_3 \cdot ZrO_2$ ternary compound.

Negas *et al*.[24] pointed out that partial reduction of Ce^{4+} to Ce^{3+} can occur above 1400°C in air. The amount of Ce^{3+}, however, seemed to be small below 1600°C, so that the ternary system ZrO_2–CeO_2–Ce_2O_3 could be regarded as the pseudobinary system ZrO_2–CeO_2 below 1600°C in air. The influence of oxygen partial pressure on the phase relation of solid solutions in Ce-Zr-O system is that the Ce^{+4} in a solid solution of ZrO_2 will be reduced to Ce^{+3} at increased temperature in reducing atmospheres (such as H2, CO, and NH4) or under a vacuum of 10^{-4} to 10^{-5} torr, or in an inert atmosphere (such as Ar and He) or in the atmosphere of flame furnaces with low oxygen partial pressure (for example, oxygen partial pressure 10^{-2} torr at 1400°C).[23,25] Cerium is the second element of the rare earth series with an electronic configuration which can be described, taking into account that of Xenon, as (Xe) $6s^2 5d^1 4f^1$. In such a configuration, the volume of 6s and 5d orbital are greater than that of the 4f orbital. Therefore, the three $6s^2$ and $5d^1$ electron are the only ones participating for chemical bonds. For this reason, the valance of the lanthanide elements in their configurations is habitually 3+.

(2) Microstructures of Ti and various sintered CeO_2/ZrO_2 samples

Figures 2(a)-(e) display the backscattered electron images of the cross-sections normal to the interfaces of Ti and various CeO_2/ZrO_2 samples after reaction at 1550°C for 4 h. Titanium is shown to the left of the micrograph, while zirconia is on the right-hand side. The vertical arrows in the upper side of individual figures indicate the original interfaces of Ti and individual CeO_2/ZrO_2 samples, respectively. The original interfaces were deliberately located according to the characteristic K_α x-ray maps of cerium (not shown), which was relatively immobile compared with respect to Zr, O, and Ti, etc. To the left of the reaction layer "I" was the α-Ti with oxygen in solid solution. Based on EDS results, the content of oxygen in α-Ti(O) was apparently decreasing with increasing amount of CeO_2. The composition of α-Ti(O) in 10Ce90Zr was measured as 70.47 at% Ti and 29.53 at% O. An α-Ti(O) in 70Ce30Zr was consisted of 85.72 at% Ti and 14.28 at% O.

Figure 2(a) and (b) indicated that extensive reactions took place at the interface between Ti and ZrO_2 containing 10 mol% and 30 mol% CeO_2. It was previously reported that needle-like α-Ti and some lamellar phases were usually found in the titanium side because of the interfacial reactions between Ti and ZrO_2.[7,8,10,11] However, only a limited reaction took place on the titanium side at the interface between Ti and those samples containing more than 50 mol% CeO_2, while pure CeO_2 reacted minimally with Ti after reaction at 1550°C for 4 h. This indicated that interfacial reactions were effectively suppressed in those samples containing more than 50 mol% CeO_2. This fact plays an important role in the engineering respect of Ti castings such that a controlled interfacial reaction results in a lower amount of α-casing and thus better

mechanical properties. Even though the system became more stable with increasing CeO_2, several reaction layers were found on the zirconia side after the interfacial reactions between Ti and various CeO_2/ZrO_2 samples. Microstructures of the reaction layers at the interface between Ti and various CeO_2/ZrO_2 samples were characterized using SEM/EDS and TEM/EDS and the results are listed in Table II. The details will be described below.

(A) Reaction layer "II" on the metal side at the Ti/10Ce90Zr and Ti/30Ce70Zr interfaces

Figure 3(a) shows the backscattered electron image (BEI) of the reaction layer "II" at the Ti/10Ce90Zr interface after reaction at 1550°C for 4 h. The reaction layer "II" consisted of the acicular α-Ti (dark) in β'-Ti (bright) matrix and the lamellar Ti_2ZrO (bright) precipitated in the α-Ti. The morphology of *α*-Ti abutted the original interface was very different from the corresponding reaction layer previously found [8,10-12] It inferred that the cause by the agglomeration of a large amount of oxygen in this region to the nearest left of the original interface. At high temperature, *α*-Ti dissolved a large amount of O and relatively a small amount of Zr, forming a metastable supersaturated solid solution *α*-Ti(O, Zr), thus resulting in the precipitation of the lamellar Ti_2ZrO during cooling. Lin and Lin[8] reported that the Ti_2ZrO lamellae were precipitated from plate-like α-Ti by a eutectoid reaction during cooling. As more zirconia was dissolved in α-Ti, the β-Ti was formed and some of them was transformed into orthorhombic β'-Ti solid solution during cooling. Figure 3(b) shows the BEI of the reaction layer "II" at the Ti/30Ce70Zr interface after reaction at 1550°C for 4 h. The reaction layer "II" consisted of *β'*-Ti (bright) and *α*-Ti (dark). In this case, no Ti_2ZrO was found in *α*-Ti (dark). It was believed that the *α*-Ti

dissolved a relatively small amount of zirconium due to much slower diffusion rate of zirconium than oxygen, thus no Ti_2ZrO precipitated in α-Ti during cooling.

(B) Reaction layer "III" on the ceramic side at the Ti/10Ce90Zr and Ti/30Ce70Zr interfaces

For the benefit of good resolution of TEM, figure 4(a) shows the TEM micrograph (bright-field image, BFI) of reaction layer "III". The reaction layer "III" was consisting of α-Ti, β'-Ti, and $Ce_2Zr_3O_{10}$ at the Ti/10Ce90Zr interface after reaction at 1550°C for 4 h. Arrow below the BFI indicates the original interface between reaction layers "II" and "III". A large amount of spherical or worm-like $Ce_2Zr_3O_{10}$ phase existed in the reaction layer "III". Fig. 4(a) also shows Ti_2ZrO lamellae precipitated in the α-Ti matrix. With the diffraction spots being indexed in Fig. 4(b), the orientation relationships of Ti_2ZrO and α-Ti were thus recognized as follows: $[110]_{Ti2ZrO}$ // $[0001]_{\alpha\text{-Ti}}$ and $(1\bar{1}0)_{Ti2ZrO}$ // $(10\bar{1}0)_{\alpha\text{-Ti}}$. The crystal structures of Ti_2ZrO and α-Ti were identified to be orthorhombic and hexagonal based upon the superimposed selected area diffraction patterns (SADPs), as shown in fig. 4(b). Figure 4(c) shows the SADP of $Ce_2Zr_3O_{10}$ phase along the zone axis of [001]. The crystal structure of $Ce_2Zr_3O_{10}$ was identified to be tetragonal from the SADP.

Figure 5(a) shows the BEI of the reaction layer "III" at the Ti/10Ce90Zr interface after reaction at 1550°C for 4 h. As 10Ce90Zr reacted with Ti at 1550°C for 4 h, an increasing amount of O and Zr from the supersaturated 10 mol% CeO_2-ZrO_2 solid solution were gradually dissolved in titanium. Because CeO_2 remained in the solid solution due to the very limited solubility of CeO_2 in Ti, the increase in the ratio

of CeO_2 to ZrO_2 gave rise to the formation of 2:3 $CeO_2 \cdot ZrO_2$ ternary compound (or $Ce_2Zr_3O_{10}$). Based on EDS results, $Ce_2Zr_3O_{10}$ consisted of 13.11 at% Ce, 20.52 at% Zr, and 66.37 at% O. The formation mechanisms of α-Ti, β'-Ti, and $Ce_2Zr_3O_{10}$ in the case of Ti/10Ce90Zr in the reaction layer "III" can be expressed as follows:

$$0.1\ CeO_2 + 0.9\ ZrO_2 \rightarrow (Ce_{0.1}Zr_{0.9})O_2 \quad \text{during sintering} \quad (1)$$

$$x\text{-Ti} + (Ce_{0.1}Zr_{0.9})O_2 \rightarrow (x\text{-Ti} + 0.75\ Zr + 1.5\ O) + Ce_{0.1}Zr_{0.15}O_{0.5} \rightarrow \alpha\text{-Ti (O, Zr)} + \beta'\text{-Ti(Zr, O)} + 0.05\ Ce_2Zr_3O_{10} \quad (2)$$

Figure 5(b) shows the BEI of the reaction layer "III" at the Ti/30Ce70Zr interface after reaction at 1550°C for 4 h. The reaction layer "III" consisted of β'-Ti (dark) and $Ce_2Zr_2O_7$ (bright). $Ce_2Zr_2O_7$ phase was dense and interconnected at the Ti/30Ce70Zr interface. The quantitative analyses of $Ce_2Zr_2O_7$ by the EDS showed that it contained 18.21 at% Ce, 18.52 at% Zr, and 63.27 at% O. This reaction mechanism can be expressed as the following equation.

$$x\text{-Ti} + Ce_2Zr_3O_{10} \rightarrow (y\text{-Ti} + Zr + 3\ O) + Ce_2Zr_2O_7 \rightarrow \beta'\text{-Ti(Zr, O)} + Ce_2Zr_2O_7 \quad (3)$$

Figure 6(a) shows the BFI of reaction layer "III" at the Ti/30Ce70Zr interface after reaction at 1550°C for 4 h. The crystal structures of $Ce_2Zr_2O_7$ and β'-Ti were identified to be cubic and orthorhombic from the SADPs as shown in Fig. 6(b) and (c) along the zone axes of [111], respectively. The $Ce_2Zr_2O_7$ has possesses the pyochlore type structure

(space group $Fd\bar{3}m$) in which one out of every eight oxygen ions is missing in the stoichiometric fluorite. The ideal $Ce_2Zr_2O_7$ structure is described as an ordered cubic close-packed array of cations (16c and 16d sites) with the oxygen ions occupying seven-eighths of the tetrahedral sites (48f and 8a sites) between the cations. The oxygen vacancies in the remaining one-eighths of the tetrahedral sites (8b site) are also ordered.

(C) Reaction layers "I" and "III" at the Ti/50Ce50Zr and Ti/70Ce30Zr interfaces

Figure 7(a) displays the BEI of reaction layers "I" and "III" at the Ti/50Ce50Zr interface after reaction at 1550°C for 4 h. Reaction layer "I" in 50Ce50Zr consisted of α-Ti, β'-Ti, and CeO_2. For comparison, as shown in Fig. 7(a) together with Fig. 2, only very few β'-Ti was found in the reaction layer "I". However, a relatively large amount of β'-Ti and α-Ti existed at the interface between Ti and ZrO_2 containing 10-30 mol% CeO_2. The reaction layer "III" in 50Ce50Zr consisted of α-Ti, β'-Ti, CeO_2, and $Ce_2Zr_2O_7$. As 50Ce50Zr reacted with Ti, a large amount of O and Zr from ZrO_2 were dissolved in titanium, giving rise to the formation of CeO_2 due to the very limited solubility of CeO_2 in Ti. From the EDS analyses, the CeO_2 in the reaction layer "III" contained 32.14 at% Ce, 64.57 at% O, and 3.29 at% Zr. The re-precipitation of CeO_2 in reaction layer "III" was dense and interconnected. It was concluded that increasing CeO_2 content was useful for better controlling the interfacial reactions. The formation mechanisms of α-Ti, β'-Ti, CeO_2, and $Ce_2Zr_2O_7$ in the case of Ti/50Ce50Zr in the reaction layer "III" can be expressed as follows:

$$0.5\ CeO_2 + 0.5\ ZrO_2 \rightarrow (Ce_{0.5}Zr_{0.5})O_2 \quad \text{durng sintering} \quad (4)$$

$$x\text{-Ti} + (Ce_{0.5}Zr_{0.5})O_2 \rightarrow (x\text{-Ti} + 0.5\ Zr + 1\ O) + 0.5\ CeO_2$$
$$\rightarrow \beta'\text{-Ti(Zr, O)} + \alpha\text{-Ti (Zr, O)} + 0.5\ CeO_2 \quad (5)$$

$$y\text{-Ti} + Ce_2Zr_3O_{10} \rightarrow (y\text{-Ti} + Zr + 3\ O) + Ce_2Zr_2O_7$$
$$\rightarrow \beta'\text{-Ti(Zr, O)} + Ce_2Zr_2O_7 \quad (6)$$

Figure 7(b) displays the BEI of reaction layers “I” and “III” at the Ti/70Ce30Zr interface after reaction at 1550°C for 4 h. Reaction layer “I” in 70Ce30Zr consisted of α-Ti, CeO_2, and $Ce_2Zr_2O_7$. For comparison, as shown in Fig. 7(b) together with Fig. 2, no β'-Ti were found in the reaction layer “I”. The reaction layer “III” in 70Ce30Zr consisted of CeO_2, $Ce_2Zr_2O_7$, and few α-Ti. The α-Ti phase was spherical and isolated at the Ti/70Ce30Zr interface. The formation mechanisms of α-Ti and CeO_2 in the case of Ti/70Ce30Zr in the reaction layer “III” can be expressed as follows:

$$0.7\ CeO_2 + 0.3\ ZrO_2 \rightarrow (Ce_{0.7}Zr_{0.3})O_2 \quad \text{durng sintering} \quad (7)$$

$$x\text{-Ti} + (Ce_{0.7}Zr_{0.3})O_2 \rightarrow (x\text{-Ti} + 0.3\ Zr + 0.6\ O) + 0.7\ CeO_2$$
$$\rightarrow \alpha\text{-Ti (Zr, O)} + 0.7\ CeO_2 \quad (8)$$

(D) Reaction layer “IV” on the ceramic side

Figures 8(a)-(d) show the BFIs of reaction layer “IV” on the ceramic side far from the original interfaces of Ti and 10Ce90Zr, 30Ce70Zr, 50Ce50Zr,

and 70Ce30Zr, respectively, after reaction at 1550°C for 4 h. Figure 8(a) shows the α-Zr particle was embedded in *c*-ZrO_{2-x} in reaction layer "IV" of 10Ce90Zr. It was believed that the oxidation-reduction reaction rather than dissolution was the predominant reaction mechanism in reaction layer "IV". The dissolution did not play a significant role, as the titanium was not detected by EDS in reaction layer "IV". It was obivous that the ZrO_{2-x} was metastable because of the extraction of oxygen from ZrO_2 by Ti. The α-Zr with oxygen in solid solution was excluded from metastable ZrO_{2-x}. However a significant increase in oxygen vacancies, as a consequence of the reaction between Ti and 30Ce70Zr, triggered the stabilization effect of zirconia. Therefore, it was inferred that the zirconia could be in the cubic phase. Figure 8(b) shows several $Ce_2Zr_2O_7$ grains were existed along the grain boundaries of *c*-ZrO_{2-x} in reaction layer "IV" of 30Ce70Zr. No α-Zr was found in the reaction layer "IV" of 30Ce70Zr. Cubic $Ce_2Zr_2O_7$ was formed due to the decomposition of the $Ce_2Zr_3O_{10}$. Since CeO_2 was completely retained in ZrO_2, no free CeO_2 was found in 10Ce90Zr and 30Ce70Zr.

Figure 8(c) shows the BFI of $Ce_2Zr_2O_7$ and dense α-Zr grain in the reaction layer "IV" of Ti/50Ce50Zr. The morphology of α-Zr in the reaction layer "IV" of Ti/50Ce50Zr was very different from 10Ce90Zr. Formation mechanisms of $Ce_2Zr_2O_7$ and α-Zr in the case of Ti/50Ce50Zr in the reaction layer "IV" can be expressed in terms of the following equation:

$$Ce_2Zr_3O_{10} \rightarrow Ce_2Zr_2O_7 + \alpha\text{-}Zr_{\text{(with O in solid solution)}} + 3O_{\text{(pariially dissolved in β'-Ti)}} \quad (9)$$

Figure 8(d) shows the BFI of reaction layer "IV" in 70Ce30Zr after

reaction at 1550°C for 4 h. Free CeO_2 existed in reaction layers “IV”. The composition of CeO_2 indicated that it contained 32.12 at% Ce, 64.99 at% O, and 2.89 at% Zr.

(3) A General Discriptions of Interfacial Reaction Layers

According to the previous discussion, the reaction layers were formed at the interface between titanium and various ceria/zirconia samples after reaction at 1550°C for 4 h (summarized in Table II). Briefly speaking, extensive reactions occurred at the interface between Ti and ZrO_2 containing 10-30 mol% CeO_2. However, interfacial reactions were effectively suppressed by incorporating more than 50 mol% CeO_2. On the metal side near the original interface, β'-Ti and Ti_2ZrO precipitated in the α-Ti matrix after Ti reacted with 10Ce90Zr, although β'-Ti and α-Ti were found for the case of 30Ce70Zr. Furthermore, only a small amount of β'-Ti was found for the case of 50Ce50Zr. No β'-Ti was found for the case of 70Ce30Zr and pure CeO_2. In the outermost ceramic region, β'-Ti and α-Ti were found along with $Ce_2Zr_3O_{10}$ in 10Ce90Zr, while β'-Ti and $Ce_2Zr_2O_7$ were found in 30Ce70Zr. Free CeO_2 existed in 50Ce50Zr and 70Ce30Zr due to a very limited solubility of CeO_2 in Ti when ZrO_2 was completely dissolved in Ti. On the ceramic side far from the original interface, spherical α-Zr was formed in addition to residual ZrO_{2-x} in 10Ce90Zr, where α-Zr was excluded from metastable ZrO_{2-x}. However, $Ce_2Zr_2O_7$ was formed in addition to residual ZrO_{2-x} in 30Ce70Zr. Dense α-Zr grains existed along the grain boundaries of $Ce_2Zr_2O_7$ in 50Ce50Zr. Free CeO_2 existed in $Ce_2Zr_2O_7$ matrix in 70Ce30Zr. However, CeO was found in 100Ce. CeO_2 was dissolved into ZrO_2 as a solid solution or reacted with ZrO_2 as $Ce_2Ze_3O_{10}$ and $Ce_2Ze_2O_7$ compound during sintering. $Ce_2Ze_2O_7$ was formed due to the reduction of Ce^{+4} ions to Ce^{+3} in ZrO_2

with low oxygen partial pressure and Ce_2O_3 reacted with ZrO_2 as a 1:2 $Ce_2O_3 \cdot ZrO_2$ ternary compound (or $Ce_2Zr_2O_7$). As 50Ce50Zr and 70Ce30Zr were reacted with Ti at 1550ºC for 4 h, CeO_2 was re-precipitated due to the strong affinity of O and Zr to Ti and the very limited solubility of CeO_2. CeO was found in the sample containing 100 mol% CeO_2 due to the oxidation-reduction between Ti and CeO_2. It was also noted that $Ce_2Ze_2O_7$ was stable and retained in the sample after reaction at 1550ºC for 4 h.

IV. Conclusions

1. The incorporation of more than 50 mol% CeO_2 significantly suppressed the interfacial reactions at the interfaces between Ti and various sintered CeO_2/ZrO_2 samples.
2. On the metal side near the original interface, a relatively large amount of β'-Ti and α-Ti were observed after Ti reacted with 10Ce90Zr or 30Ce70Zr at 1550ºC for 4 h. However, few β'-Ti was found after Ti reacted with 50Ce50Zr. No β'-Ti was found after Ti reacted with 70Ce30Zr or CeO_2 at 1550ºC for 4 h.
3. After reaction at 1550ºC for 4 h, β'-Ti, α-Ti and $Ce_2Zr_3O_{10}$ were found in the outermost region of 10Ce90Zr, while β'-Ti and $Ce_2Zr_2O_7$ existed in the outermost region of 30Ce70Zr. The formation of $Ce_2Zr_3O_{10}$ was caused by the extensive dissolution of ZrO_2 in Ti together with a very limited solubility of CeO_2. The formation of $Ce_2Zr_2O_7$ was caused by the outward diffusion of O and Zr from $Ce_2Zr_3O_{10}$ in Ti.
4. The CeO_2 was re-precipitated in the outermost region of 50Ce50Zr

and 70Ce30Zr after reaction at 1550ºC for 4 h. This was due to the strong Ti affinity of O and Zr.

5. It was also noted that $Ce_2Ze_2O_7$ was stable and retained in the sample containing more than 30 mol% CeO_2 after reaction at 1550ºC for 4 h.

References

[1]B. C. Weber, W. M. Thompson, H. O. Bielstein, and M. A. Schwartz, "Ceramic Crucible for Melting Titanium," *J. Am. Ceram. Soc.*, **40** [11] 363-73 (1957).

[2]R. Ruh, "Reaction of Zirconia and Titanium at Elevated Temperatures," *J. Am. Ceram. Soc.*, **46** [7] 301-06 (1963).

[3]R. L. Saha, T. K. Nandy, R. D. K. Misra, and K. T. Jacob, "Evaluation of the Reactive of Titanium with Mould Materials during Casting," *Bull. Mater. Sci.*, **12** [5] 481-93 (1989).

[4]R. L. Saha and R. D. K. Misra, "Formation of low-melting eutectic at the metal-mould interface during titanium casting in zircon sand moulds," *J. Mater. Sci. Lett*, **10** 1318-19 (1991).

[5]K. I. Suzuki, S. Watakabe, and K. Nishikawa, "Stability of Refractory Oxides for Mold Material of Ti-6Al-4V Alloy Precision Casting," *J. Jpn. Inst. Met.*, **60** [8] 734-43 (1996).

[6]K. F. Lin and C. C. Lin, "Interfacial Reactions between Ti-6Al-4V Alloy and Zirconia Mold During Casting," *J. Mater. Sci.*, **34** 5899-906 (1999).

[7]K. F. Lin and C. C. Lin, "Transmission Electron Microscope Investigation of the Interface between Titanium and Zirconia," *J. Am. Ceram. Soc.*, **82** [11] 3179-85 (1999).

[8]K. L. Lin and C. C. Lin, "Ti_2ZrO Phases Formed in the Titanium and

Zirconia Interface after Reaction at 1550oC," *J. Am. Ceram. Soc.*, **88** [5] 1268-72 (2005).

[9]K. L. Lin and C. C. Lin, "Zirconia-Related Phases in the Zirconia/Titanium Diffusion Couple after Annealing at 1100o to 1550oC," *J. Am. Ceram. Soc.*, **88** [10] 2928-34 (2005).

[10]K. L. Lin and C. C. Lin, "Microstructural Evolution and Formation Mechanism of the Interface Between Titanium and Zirconia Annealed at 1550oC," *J. Am. Ceram. Soc.*, **89** [4] 1400-8 (2006).

[11]K. L. Lin and C. C. Lin, "Effects of Annealing Temperature on Microstructural Development at the Interface Between Zirconia and Titanium," *J. Am. Ceram. Soc.*, **90** [3] 893-9 (2007).

[12]C. C. Lin, Y. W. Chang, and K. L. Lin, "Effect of Yttria on Interfacial Reactions Between Titanium Melt and Hot-Pressed Yttria/Zirconia Composites at 1700oC," *J. Am. Ceram. Soc*, **91** [7] 2321-27 (2008).

[13]K. Tsukuma and M. Shimada, "Strength, Fracture Toughness and Vickers Hardness of CeO_2-Stabilized Tetragonal ZrO_2 Polycrystals (Ce-TZP)," *J. Mater. Sci.*, **20** [4] 1178-84 (1985).

[14]K. Tsukuma, "Mechanical Properties and Thermal Stability of CeO_2 Containing Tetragonal Zirconia Polycrystals," *Am. Ceram. Soc. Bull*, **65** [10] 1386-89 (1986).

[15]J. G. Duh, H. T. Dai, and B. S. Chiou, "Sintering Microstructure, Hardness, and Fracture Toughness Behaviour of Y_2O_3-CeO_2-ZrO_2," *J. Am. Ceram. Soc*, **71** [10] 813-19 (1988).

[16]S. B. Bhaduri, A. Chakraborty, and R. M. Rao, "Method of Fabrication Ceria-Stabilized Tetragonal Zirconia Polycrystals," *J. Am. Ceram. Soc*, **71** [9] C-410-C-11 (1988).

[17]J. Wang, X. H. Zheng, and R. Stevens, "Fabrication and Microstructure-Mechanical Property Relationships in Ce-TZPs," *J. Mater. Sci.*, **27** [19] 5348-56 (1992).

[18]G. Cliff and G. W. Lorimer, "The Quantitative Analysis of Thin Specimens," *J. Microsc.*, **130** [3] 203-07 (1975).

[19]S. Roitti and V. Longo, "Investigation of Phase Equilibrium Diagrams Among Oxides by means of Electrical Conductivity Measurements. Application of the Method to the System CeO_2-ZrO_2," *Ceramurgia Int.*, **2** [2] 97-102 (1972).

[20]V. Longo and D. Minichelli, "X-Ray Characterization of $Ce_2Zr_3O_{10}$," *J. Am. Ceram. Soc*, **56** [11] 600 (1973).

[21]E. Tani, M. Yoshimura, and S. Somiya, "Revised Phase Diagram of the System ZrO_2-CeO_2 Below 1400oC," *J. Am. Ceram. Soc*, **66** [7] 506-10 (1983).

[22]T. Sasaki, Y. Ukyo, K. Kuroda, S. Arai, S. Muto, and H. Saka, "Crystal

Structure of $Ce_2Zr_2O_7$ and -$Ce_2Zr_2O_{7.5}$," *J. Ceram. Soc. Japan*, **112** [8] 440-44 (2004).

[23]Z. C. Kang, "Phases in $Ce_{0.5}Zr_{0.5}O_{2-x}$ System," *J. Alloys and Compounds*, **408-12** 1103-07 (2006).

[24]T. Negas, R. S. Roth, C. L. McDaniel, H. S. Parker, and C. D. Olson, "Influence of K_2O on the Cerium Oxide-ZrO_2 System," 605-14 (1976).

[25]T. Xu, P. Wang, P. Fang, Y. Kan, L. Chen, V. Jef, V. D. B. Omer, and V. L. Jef, "Phase Assembly and Microstructure of CeO_2-doped ZrO_2 Ceramics Prepared by Spark Plasma Sintering," *J. Eur. Ceram. Soc*, **25** [15] 3437-42 (2005).

計畫成果自評部份

原申請計劃不同組成的鎂安定氧化鋯燒失率過高，且不易得到緻密性的鎂安定氧化鋯塊材，造成後續跟 Ti 進行高溫擴散介面反應的困難，因此將安定劑選擇換成氧化鈰(CeO_2)，由 XRD 的分析結果發現陶瓷(CeO_2/ZrO_2)燒結試片中 CeO_2 會有+4 價 Ce 轉換成+3 價 Ce 的現象，而此現象在 ZrO_2 添加其它的安定劑(Y_2O_3，CaO)中並不會發生。不同組成的鈰安定氧化鋯塊材在跟 Ti 進行高溫擴散介面反應後，微觀結構有極大的不同，本實驗嘗試以 X-ray 繞射儀、FESEM/EDS、TEM/EDS 等分析鈦金屬與陶瓷間反應介面之微觀結構，並探討 CeO_2 含量對 CeO_2/ZrO_2 陶瓷複合材料與 Ti 金屬高溫擴散介面反應的影響，期以獲得最佳的 CeO_2/ZrO_2 比例，對應用於鈦合金鑄造的坩堝/陶模材料有極大貢獻。

第一年實驗進行以 X-ray 繞射儀及熱場發射掃瞄式電子顯微鏡及能量分散能譜儀（FESEM/EDS）來分析鈦金屬與 CeO_2/ZrO_2 陶瓷間反應介面之微觀結構，XRD 與 FESEM/EDS 之分析皆以完成。

第二年實驗進行預計以 TEM/EDS 來分析不同介面試片中個別反應層的反應相並合理推測出每個反應相的生成機構。

預計把本實驗所獲得的重要結果發表在美國陶瓷學會期刊上。

Table I. Designations, Compositions, Sintering Conditions, Relative Densities and XRD Phases of CeO_2/ZrO_2 Samples

Specimens	Composition (mol%)	Sintering conditions	Relative Densities	XRD Phases
10Ce90Zr	10% CeO_2 + 90% ZrO_2	1400℃/4 h/Air	98.9%	*t*-ZrO_2, *m*-ZrO_2
30Ce70Zr	30% CeO_2 + 70% ZrO_2	1400℃/4 h/Air	99.3%	*c*-ZrO_2, *t*-ZrO_2, *m*-ZrO_2 $Ce_2Zr_3O_{10}$, $Ce_2Zr_2O_7$
50Ce50Zr	50% CeO_2 + 50% ZrO_2	1400℃/4 h/Air	99.1%	*c*-ZrO_2, *t*-ZrO_2, *m*-ZrO_2 $Ce_2Zr_3O_{10}$, $Ce_2Zr_2O_7$
70Ce30Zr	70% CeO_2 + 30% ZrO_2	1400℃/4 h/Air	98.8%	$Ce_2Zr_2O_7$, *c*-ZrO_2
100Ce	100% CeO_2	1400℃/4 h/Air	99.5%	*c*-CeO_2

Table II. Reaction Layers Formed at the Interfaces of Ti and CeO_2/ZrO_2 Samples after Reaction at 1550°C/4 h

Specimens	**mol% CeO_2**	**Interface reaction layers and phases**				**Reaction layer "IV" in the Ceramic side**
		Ti side		**Ceramic side**		
10Ce90Zr	10 mol%	I	α-Ti + Ti_2ZrO	III	α-Ti + β′-Ti + $Ce_2Zr_3O_{10}$	*c*-ZrO_{2-x}, α-Zr
		II	α-Ti + Ti_2ZrO + β′-Ti			
30Ce70Zr	30 mol%	I	α-Ti + Ti_2ZrO	III	β′-Ti + $Ce_2Zr_2O_7$	*c*-ZrO_{2-x}, $Ce_2Zr_2O_7$
		II	α-Ti + β′-Ti			
50Ce50Zr	50 mol%	I	CeO_2 + β′-Ti	III	CeO_2, α-Ti + β′-Ti + $Ce_2Zr_2O_7$	$Ce_2Zr_2O_7$, α-Zr
70Ce30Zr	70 mol%	I	CeO_2 + $Ce_2Zr_2O_7$	III	CeO_2, α-Ti + $Ce_2Zr_2O_7$	$Ce_2Zr_2O_7$, CeO_2
100Ce	100 mol%	I	α-Ti + CeO	III	α-Ti + CeO	CeO

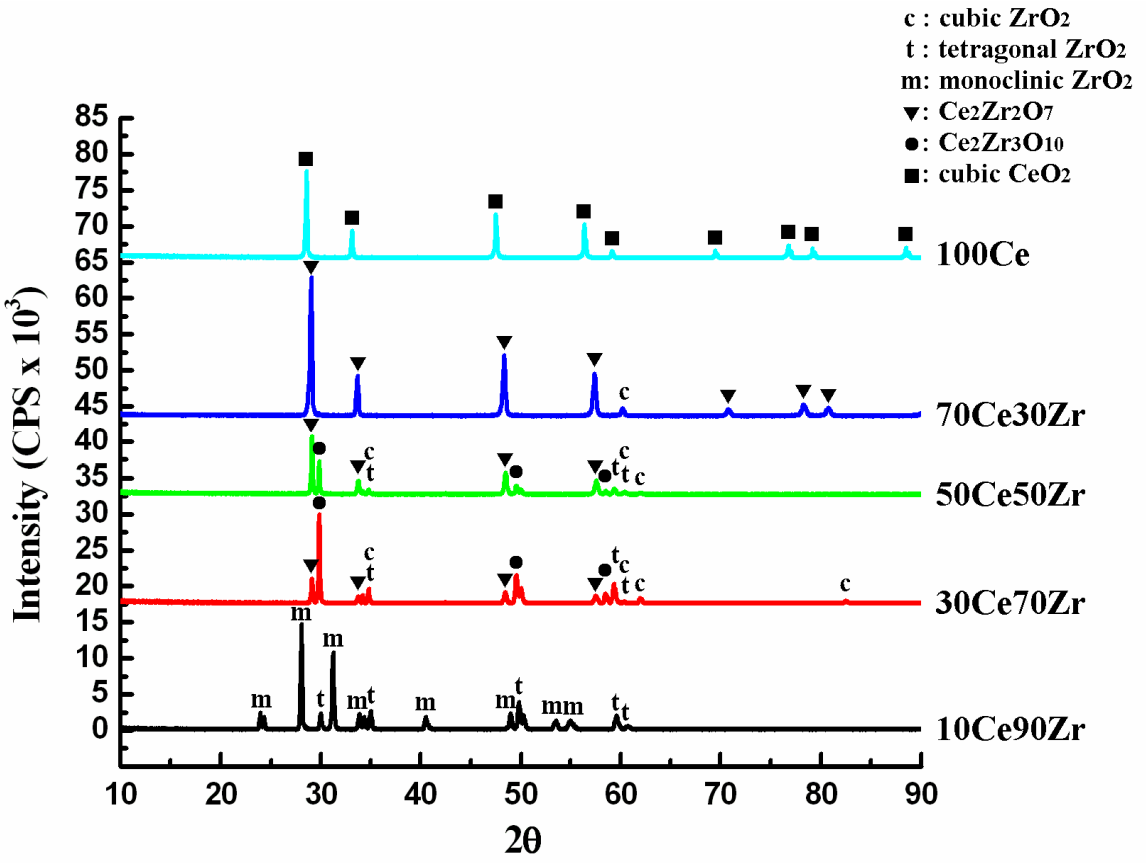

Fig. 1. X-ray diffraction spectra of various sintered CeO_2/ZrO_2 samples.

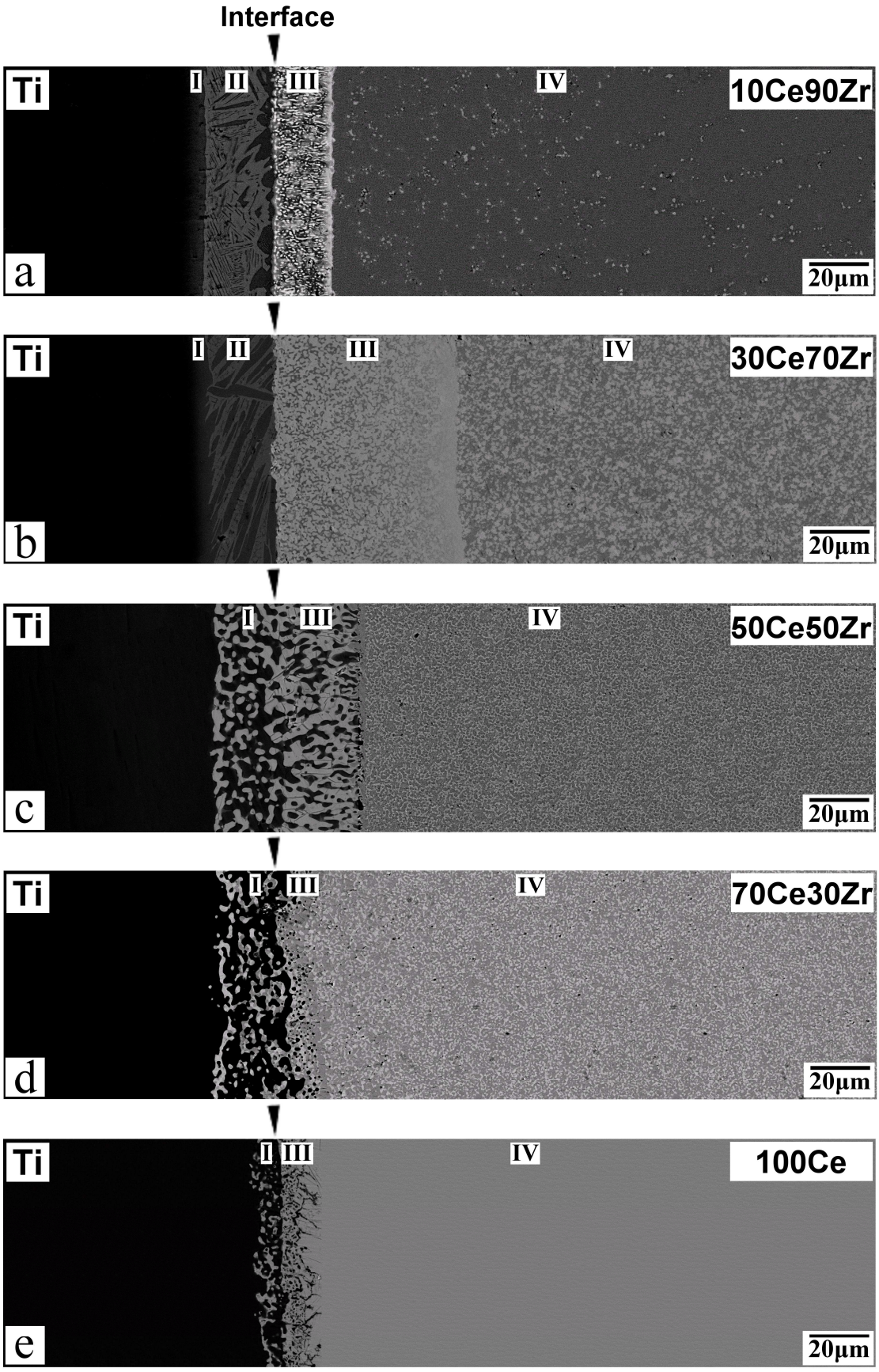

Fig. 2. **(a)-(e)** The backscattered electron images of the cross section between Ti

and CeO_2/ZrO_2 samples after reaction at 1550°C for 4 h. The arrows indicate the original interfaces between Ti and CeO_2/ZrO_2 samples.

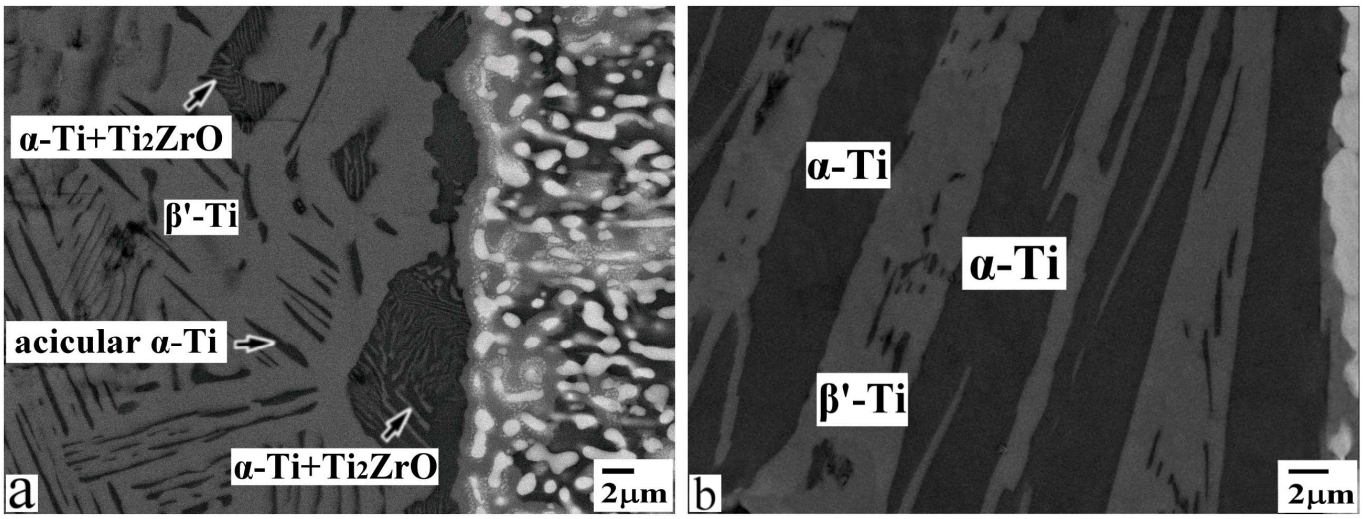

Fig. 3. The backscattered electron images of reaction layer "II" in the titanium side at the interface between (a) Ti and 10Ce90Zr and (b) Ti and 30Ce70Zr after reaction at 1550°C for 4 h.

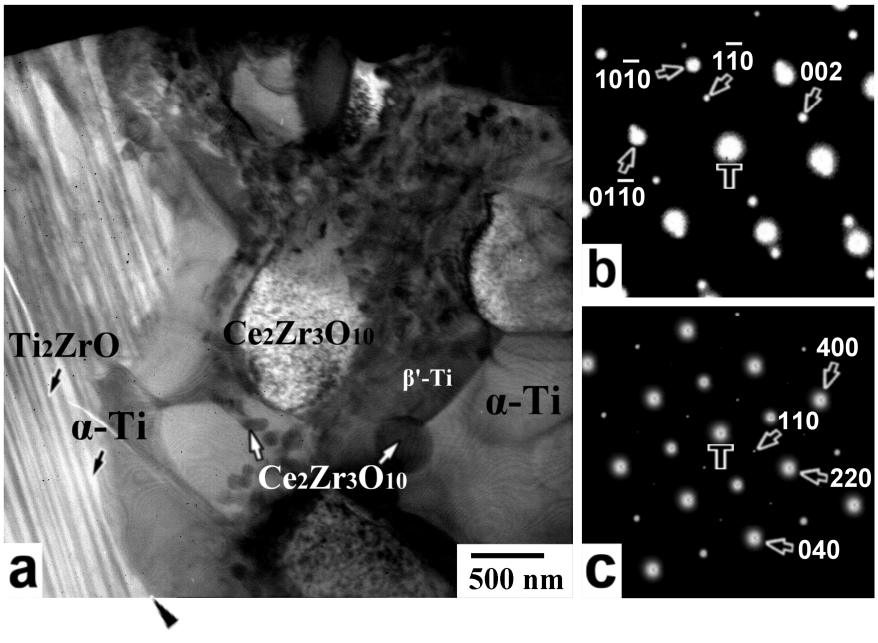

Fig. 4. (a) The bright-field image of reaction layers "II" and "III" at the interface between Ti and 10Ce90Zr after reaction at 1550°C for 4 h; (b) selected area diffraction patterns of the lamellar Ti_2ZrO and α-Ti, Z = $[0001]_{\alpha\text{-}Ti}$ //$[110]_{Ti2ZrO}$; (c) a selected area diffraction pattern of the $Ce_2Zr_3O_{10}$ with the zone axis [001]. Arrow below the bright-field image indicates the interface of reaction layers "II" and "III".

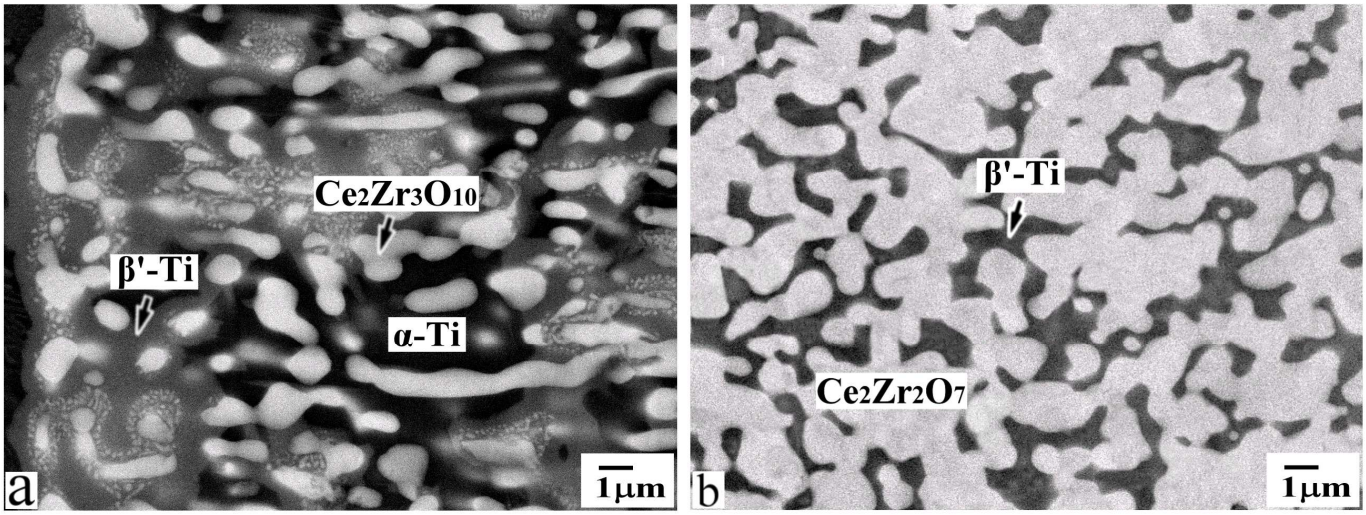

Fig. 5. The backscattered electron images of reaction layer "III" in the zirconia side near the original interface between (a) Ti and 10Ce90Zr and (b) Ti and 30Ce70Zr after reaction at 1550°C for 4 h.

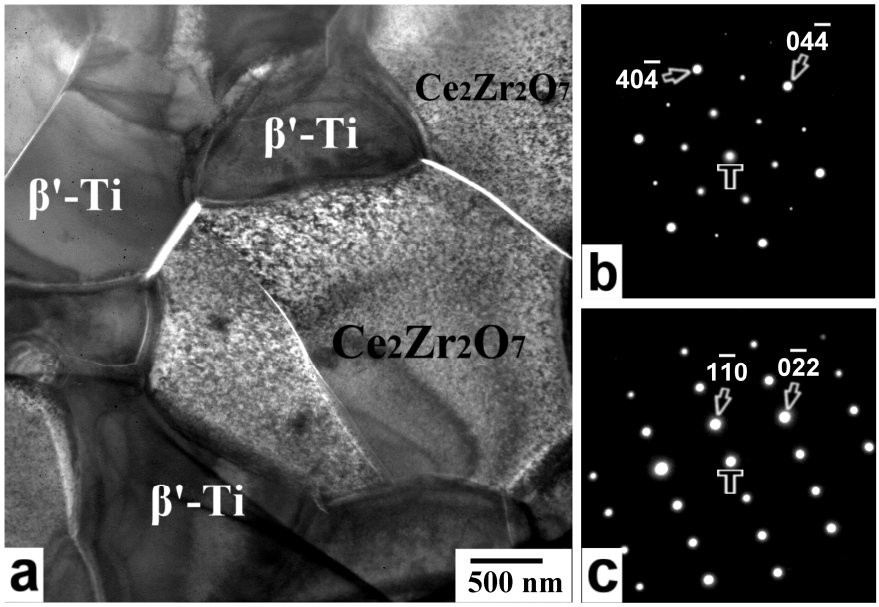

Fig. 6. (a) The bright-field image of reaction layer “III” at the interface between Ti and 30Ce70Zr after reaction at 1550°C for 4 h; (b) selected area diffraction patterns of the
$Ce_2Zr_2O_7$ with the zone axis [111].; (c) a selected area diffraction pattern of the β′-Ti with the zone axis [111].

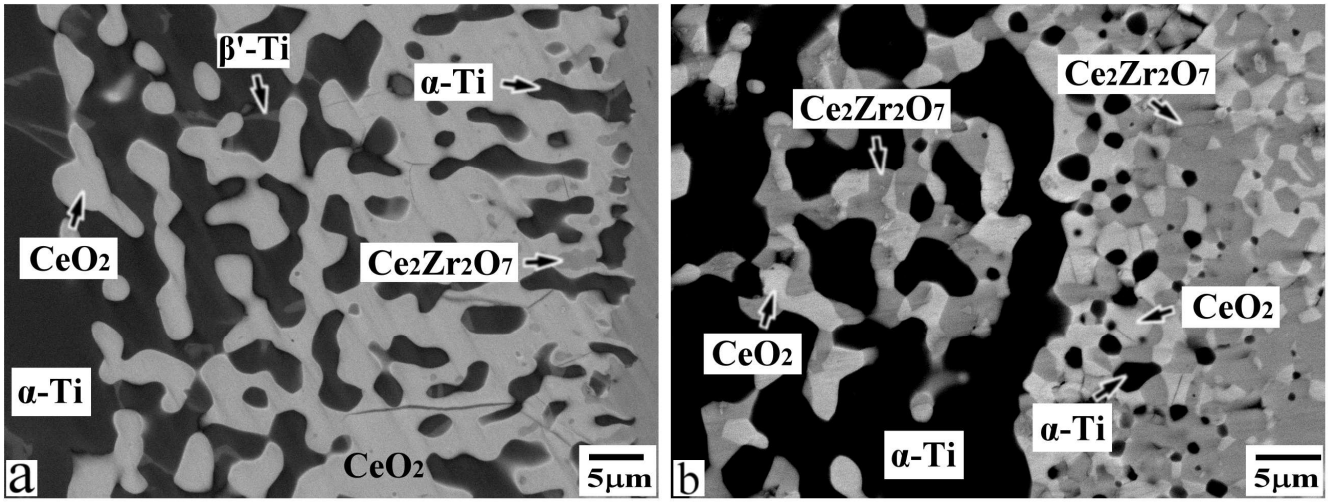

Fig. 7. The backscattered electron images of reaction layer "I" and "III" at the interface between (a) Ti and 50Ce50Zr and (b) Ti and 70Ce30Zr after reaction at 1550°C for 4 h.

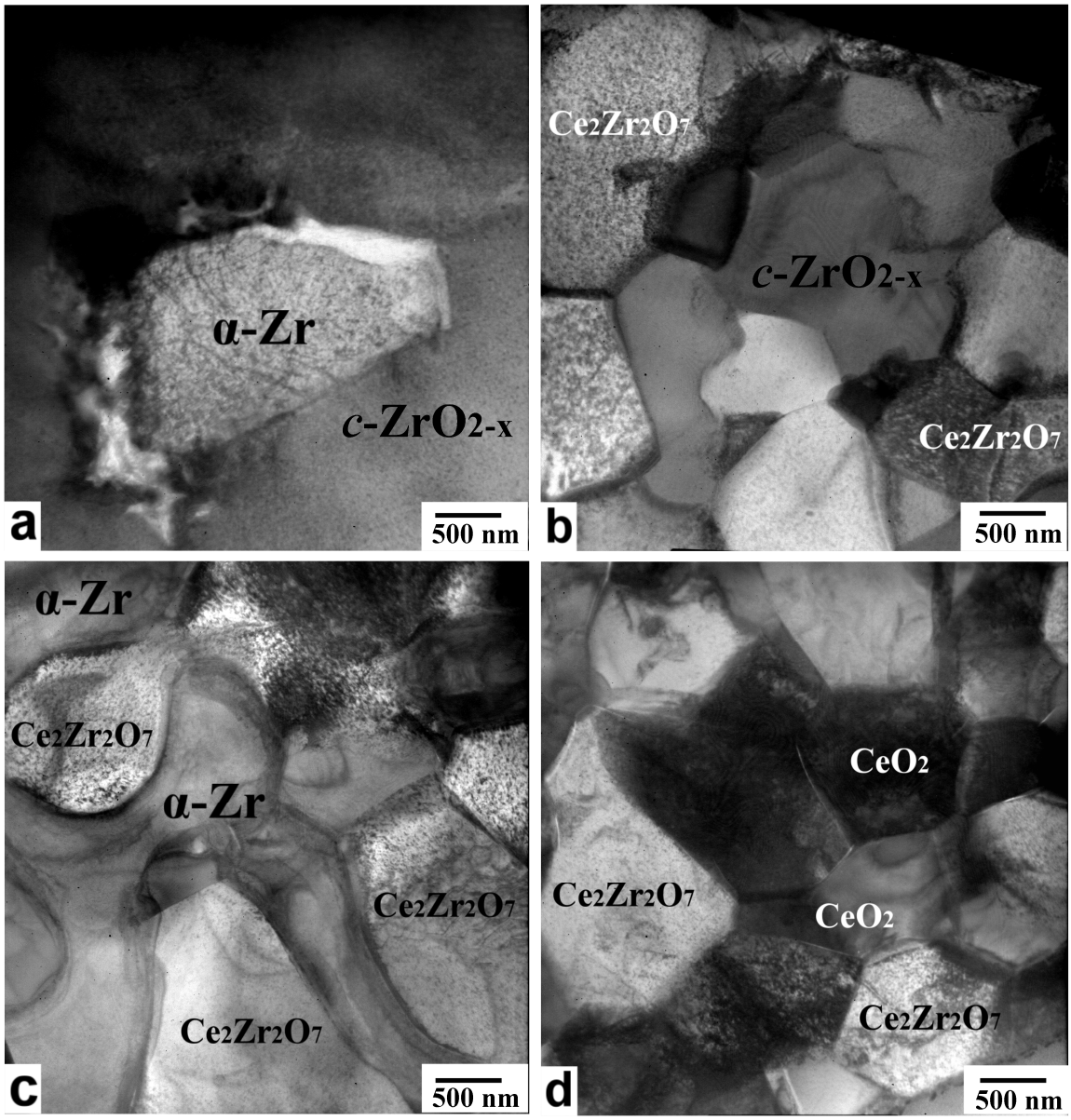

Fig. 8. The bright-field images of reaction layer "IV" in the zirconia side far away from the interface between (a) Ti and 10Ce90Zr, (b) Ti and 30Ce70Zr, (c) Ti and 50Ce50Zr, and (d) Ti and 70Ce30Zr after reaction at 1550°C for 4 h.